Bone Reports 10 (2019) 100202

Contents lists available at ScienceDirect

Bone Reports

journal homepage: www.elsevier.com/locate/bonr

Relaxin 2 carried by magnetically directed liposomes accelerates rat midpalatal suture expansion and subsequent new bone formation

Hiroyuki Kamimoto, Yukiho Kobayashi*, Keiji Moriyama

Maxillofacial Orthognathics, Department of Maxillofacial Reconstruction and Function, Division of Maxillofacial/Neck Reconstruction, Graduate School of Medical and Dental Sciences, Tokyo Medical and Dental University, 1-5-45, Yushima, Bunkyo-ku, Tokyo 113-8549, Japan

ARTICLE INFO

Keywords:
Suture expansion
Relaxin
Liposome
Drug delivery system
In vivo imaging

ABSTRACT

Relaxin (RLN) is an insulin-like peptide hormone that enables softening and lengthening of the pubic symphysis and uterine cervix. Here, we analyzed the effects of RLN2 on the expansion of rat midpalatal suture (MPS) using a magnetically directed liposome-based drug delivery system. Thirty-six male rats were divided into three groups: control (MPS was not expanded), lipo (expanded for 1 week with vehicle liposomes encapsulating ferric oxide and Cy5.5), and RLN-lipo (expanded for 1 week with the liposomes coated with RLN2). Rats were sacrificed after 1 week of expansion or after 2 weeks of retention. To accumulate RLN2-liposomes, a magnetic sheet was fixed to the palatal mucosa of the MPS. *In vivo* imaging showed magnetically controlled accumulation of liposomes in the MPS for 72 h. Immunohistochemistry revealed RLN2 expression in the MPS after expansion and relaxin receptor (RXFP) 2 expression at the osteogenic front (OF) in the RLN-lipo group; all groups expressed RXFP1 in the MPS. MPS expansion and bone formation were significantly accelerated at the OF in RLN-lipo group compared with the other groups. In the RLN-lipo group, significantly accelerated serrate bone deposition and elevated periostin (POSTN), iNOS, and MMP-1 levels were observed in the MPS. Sclerostin (SOST) expression was significantly reduced in newly formed bone in the RLN-lipo group. Our data revealed that RLN2 enhanced suture expansion *via* MMP-1 and iNOS secretion in the sutural fibroblasts and new bone formation *via* POSTN expression in osteoblasts at the OF. These properties may be useful for developing a new less-invasive orthopedic treatment aiming at sutural modification of cranio- and maxillofacial deformity patients.

1. Introduction

Relaxin (RLN) is a pleiotropic hormone of the insulin-like peptide hormone family that is well known to facilitate parturition by inducing the softening and lengthening of the pubic symphysis and softening of the cervix during the peripartum period (Lu et al., 2005). Among members of this family, RLN, insulin-like peptide (INSL) 3, and INSL5 interact with relaxin family peptide receptors (RXFPs) 1–4 (Bathgate et al., 2013; Bathgate et al., 2005; Bathgate et al., 2006). The anti-fibrotic effects of human-gene 2 (H2) relaxin (serelaxin), which is structurally related to INSL3, promote the secretion of collagen-degrading MMPs *via* RXFP1/ERK1/2 signaling in fibroblasts and myofibroblasts following kidney injury in rats and in rat renal myofibroblasts (Mookerjee et al., 2009).

In osteoblast progenitor cells, RXFP2/INSL3 signaling induces alkaline phosphatase (ALP) activity, extracellular matrix mineralization, and mitogen-activated kinase (MEK) and ERK1/2 activation (Ferlin et al., 2011). Ferlin et al. reported that 64% of young men with mutated RXFP2 (T222P) had significantly lower bone mass density (Ferlin et al., 2008). Moreover, RXFP2-deficient mice showed decreases in bone mass, mineralizing surface, bone formation (Ferlin et al., 2008), thus, INSL3/RXFP2 signaling was found to be involved in bone metabolism. In our previous study, we reported the expression pattern of *Rxfp1* and *Rxfp2* mRNAs during mouse craniofacial bone and tooth development (Duarte et al., 2014b) and found that RLN inhibited collagen deposition by inhibiting ColIa1 expression and inducing MMPs secretion into the culture medium of MC3T3-E1 through Rxfp2 using siRNA targeting *Rxfp1* and *Rxfp2*, and concluded that administration of RLN enhanced osteoblastic differentiation, mineralization, and extracellular matrix degradation *in vitro* through RXFP2 (Duarte et al., 2014a). Moon et al. showed that RLN enhanced bone morphogenetic protein (BMP) 2-induced bone formation and osteoblast differentiation by upregulation of runt-related transcription factor 2 (*Runx2*) expression and activity (Moon et al., 2014).

Liposomes have a lipid bilayer with an internal aqueous cavity and have been investigated as a drug delivery system because of their lack

* Corresponding author.
E-mail addresses: h-kamimoto.mort@tmd.ac.jp (H. Kamimoto), yukiho-kobayashi.mort@tmd.ac.jp (Y. Kobayashi), k-moriyama.mort@tmd.ac.jp (K. Moriyama).

https://doi.org/10.1016/j.bonr.2019.100202
Received 6 November 2018; Received in revised form 6 February 2019; Accepted 11 March 2019
Available online 14 March 2019

of toxicity and ease of synthesis. Matsuo et al. reported that magnet-controlled liposomes with human recombinant BMP-2 are effective for bone defect healing in a rat bone defect model (Matsuo et al., 2003). Application of liposome-based drug delivery systems in the craniofacial region are now being examined using various animal models (Baccaglini et al., 2001; He et al., 2015) and in human patients (Barron et al., 2005). As a preliminary study, our group reported that administration of RLN-liposomes enhanced the expansion of mouse calvarial sagittal sutures and bone remodeling at the parietal bones (Duarte et al., 2017).

In this study, we aimed to achieve transmucosal magnetic control of the *in vivo* localization of RLN2 carried by liposomes during lateral expansion of the rat midpalatal suture (MPS). We show that RLN2 enhanced MPS expansion with MMP-1 and iNOS expression and significantly promoted subsequent new bone formation with POSTN expression. The results of this study highlight the therapeutic properties of RLN2 for the orthopedic treatment of craniofacial and maxillofacial sutures.

2. Materials and methods

2.1. Reagents and animals

Thirty-six 12-week-old inbred Crl: SD male rats were divided into three groups: control (MPS was not expanded, appliances were adjusted passively, magnetic sheets were fixed and liposomes were not injected), Vehicle (MPS was expanded for 1 week, treated with vehicle liposomes encapsulating ferric oxide and fluorescent Cy5.5 dye), and RLN-lipo groups (MPS was expanded for 1 week, treated with the liposomes coated with RLN2). Groups were subdivided into the expansion group, which were sacrificed after the 1-week expansion, and the retention group, which were sacrificed at 2 weeks after expansion (Fig. 1A). All animal experiments were performed in accordance with protocols approved by the Institutional Animal Care and Use Committee of Tokyo Medical and Dental University (A2017-102). Bilayer cholesterol liposomes (diameter < 100 nm) containing nanometer-sized magnetite (ferric oxide) particles for magnetic control of liposome accumulation and the fluorescent dye Cy5.5 for experimental *in vivo* imaging were used to localize recombinant human RLN2 protein (R&D Systems, Minneapolis, MN, USA) to the rat MPS. Liposomes containing 29.9 μg/mL RLN2 were developed by Glycolipo (Katayama Chemical, Osaka, Japan) as described previously (Duarte et al., 2014a). In the RLN-lipo group, RLN2 was administered at a dose of 100 ng. Rats were anesthetized, and a helical expansion spring made of a 0.014-inch stainless steel wire (Tomy international, Tokyo, Japan) was placed between the upper incisors using a ligature wire (Tomy international) with light cured resin (Transbond; 3M Unitek, St. Paul, MN, USA) (Fig. 1B). The expansion force was adjusted to 50 gf using a tension gauge. In the retention group, upper incisors were fixed with light-cured resin after expansion, to prevent relapse. After anesthesia, RLN2-liposomes or liposomes alone were injected into the palatal mucosa just over the MPS every 48 h with a syringe (microliter syringes with 22 G needle; HAMILTON, Nevada, USA). To localize RLN2 at the MPS, Nd-Fe-B magnet sheet (2.0 mm in width, 8.0 mm in length, 1.0 mm in thickness, surface magnet force was 100 mT; Magna, Tokyo, Japan) was secured with sutures to the palatal mucosa, just over the MPS (Fig. 1B). Four rats of each group were intraperitoneally injected with tetracycline hydrochloride (20 mg/kg; Sigma-Aldrich) on day 0 and calcein (20 mg/kg; Sigma-Aldrich, St. Louis, MO, USA) on day 5 for bone double labeling (Fig. 1A).

2.2. Three-dimensional (3D) micro-computed tomography (CT) analysis

Samples were stored in ethanol and scanned at 85 kV, 85 μA, and 0.02 mm/voxel, with filtration through a 0.1 mm brass plate using a high-resolution X-ray μCT system (SMX-100CT; Shimadzu, Kyoto, Japan). The adoptive threshold was adjusted with 3D image analysis software (TRI/3-D-BON; Ratoc, Osaka, Japan).

2.3. In vivo imaging of liposomes

To investigate the duration of RLN2-liposomes in the MPS during expansion, a preliminary test was performed (Fig. 2A). MPS expansion was performed with an RLN2-liposome injection, with or without a magnet sheet. After anesthesia, Rats were fixed in supine position with its mouth open. To visualize the localization of RLN2-liposomes, the fluorescence signal from Cy5.5 was detected with an *in vivo* imaging system (exposure time: 1.0 s; field of view: 10 cm × 10 cm; subject height: 2.0 cm; binning: medium, IVIS Lumina XRMS; Summit Pharmaceuticals International, Tokyo, Japan) up to 92 h every 24 h after RLN2-lipo injection.

2.4. Histological analysis of the MPS

Rat maxillary bones were dissected and frozen in hexane cooled with carbon dioxide, followed by embedding in the media (Supercryo-embedding medium, SCEM; Leica Microsystems, Wetzlar, Germany). SCEM frozen blocks were covered with adhesive film (Cryofilm Type 2C; Leica) and coronally sectioned with the film at 5 μm intervals. Sections were then fixed in 10% neutral buffer formalin solution and stained with Mayer's hematoxylin and eosin. ALP activity was evaluated using a TRAP-ALP staining kit (Wako). To visualize bone double labeling, rat maxillary bones were dissected, fixed with 70% ethanol, and dehydrated in an ethanol series. Samples were then embedded with methyl methacrylate resin (Technovit9100; Heraeus-Kulzer, Hanau, Germany) and coronally sectioned every 40 μm (Kureha Special Laboratory, Tokyo, Japan). Sections were stained with toluidine blue and observed under an inverted optical microscope (Axiovert 200M; Carl Zeiss, Jena, Germany) using Axio Vision software (version 4.8; Carl Zeiss). The number of nuclei was counted on HE-stained images, at the suture, the osteogenic front, and the newly formed bone area (1000 × 1000-pixel box over the MPS).

2.5. Immunohistochemistry (IHC) and fluorescent immunostaining

IHC was performed using anti-RLN2 (LS-B10495; LifeSpan BioSciences, Seattle, WA, USA), anti-RXFP1 (CB-18419; Proteintech, Rosemont, IL, USA), anti-RXFP2 (NLS4753; Novus Biologicals, Littleton, CO, USA), and anti-periostin antibodies (ab14041; Abcam, Cambridge, UK). Specimens were then incubated with anti-mouse/rabbit IgG antibodies provided with the ImmPRESS UNIVERSAL REAGENT kit (Vector Laboratories, Burlingame, CA, USA). The reaction was developed with Histofine Simple Stain DAB (Nichirei Biosciences, Tokyo, Japan) and counterstained with methyl green or hematoxylin. For fluorescent immunostaining, we used anti-MMP-1 (aa169–464, FITC, LS-C418498C418498; LifeSpan), anti-iNOS (2072R-FITC; Bioss, MA, USA), and anti-sclerostin (SOST) antibodies (AF1589, R&D Systems). Secondary antibodies for SOST were Alexa Fluor 488 rabbit anti-goat IgG (H + L) (A-11078; Invitrogen). Samples were mounted with ProLong Diamond Antifade Mount with DAPI (Thermo Fisher Scientific, MA, USA). DAB-positive areas were measured using NIH image software.

2.6. Statistical analysis

Differences in quantitative data were determined by Kruskal Wallis H-tests followed by Mann-Whitney *U* tests with Bonferroni correction because of the sample size limitation. Data are expressed with the median value, and differences with p values lower than 0.05 were considered significant.

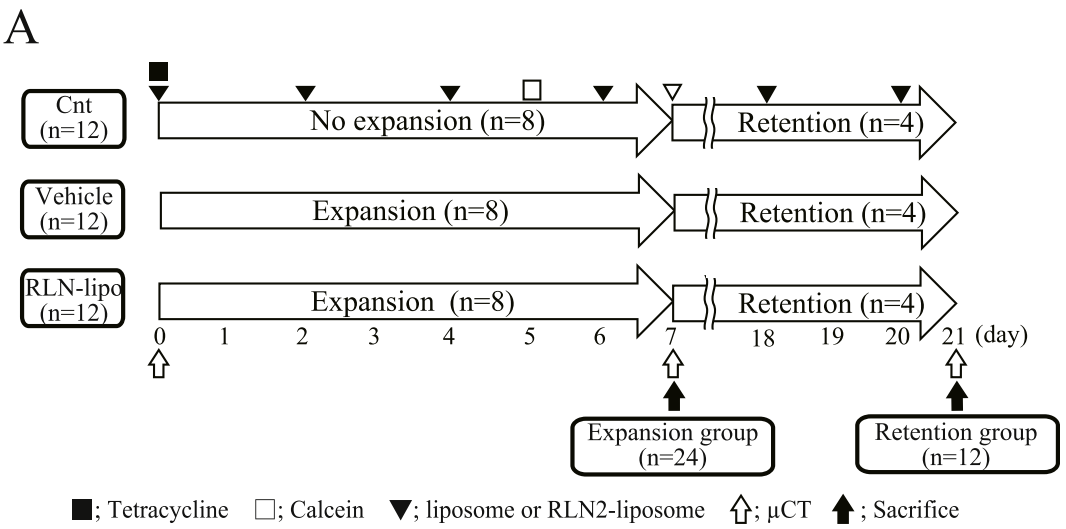

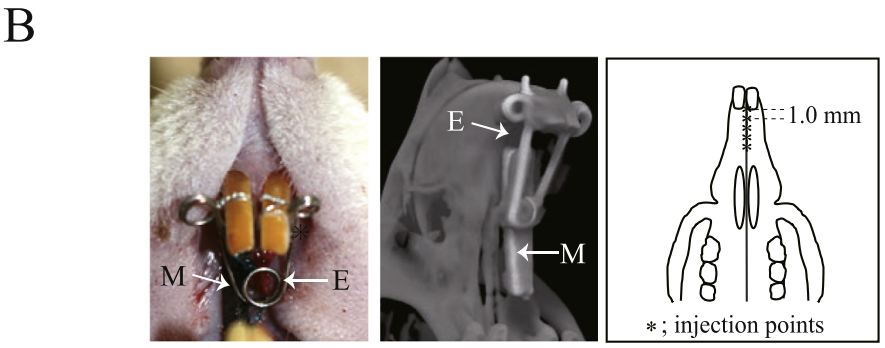

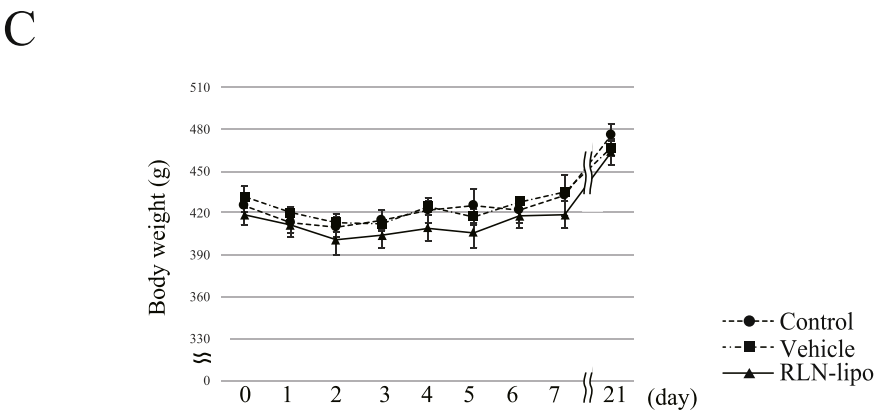

Fig. 1. Experimental protocol of palatal expansion and application of RLN2.
(A) Schematic illustration of the experimental time course. Injection of liposome or RLN2-liposome into the palatal mucosa just over the midpalatal suture (MPS) was performed every 48 h (closed arrowheads). (B) Representative photograph of the MPS expansion fixed on the maxillary incisors of the rat, and micro-CT image of the rat maxillary area with the expansion appliance (E) and magnetic sheet (M). Closed arrowheads indicate injection points at intervals of 1.0 mm. (C) Body weights of rats in each group during the expansion and retention periods.

3. Results

3.1. In vivo accumulation of RLN2-liposomes by magnetic accumulation during MPS expansion

During the experimental period, particularly from days 2 to 5, slight decreases in body weight were observed in all groups, but no significant differences were observed between the control, the vehicle, and RLN-lipo groups (Fig. 1C). At the end of the experimental period (day 21), all groups showed weight gains (Fig. 1C). From a preliminary investigation, liposomes were present in the palatal mucosa, as shown by *in vivo* imaging. Without magnet sheets, liposomes disappeared within 48 h of expansion, but remained present from 48 to 72 h after expansion (Fig. 2A). Therefore, we injected liposomes and RLN2-containing liposomes every 48 h. We determined the concentration of RLN2 in the venous blood of rats in the RLN-lipo group. Enzyme-linked immunosorbent assays were not successful (data not shown); however, IHC after 7 days of expansion (Fig. 2B) showed intense positive areas

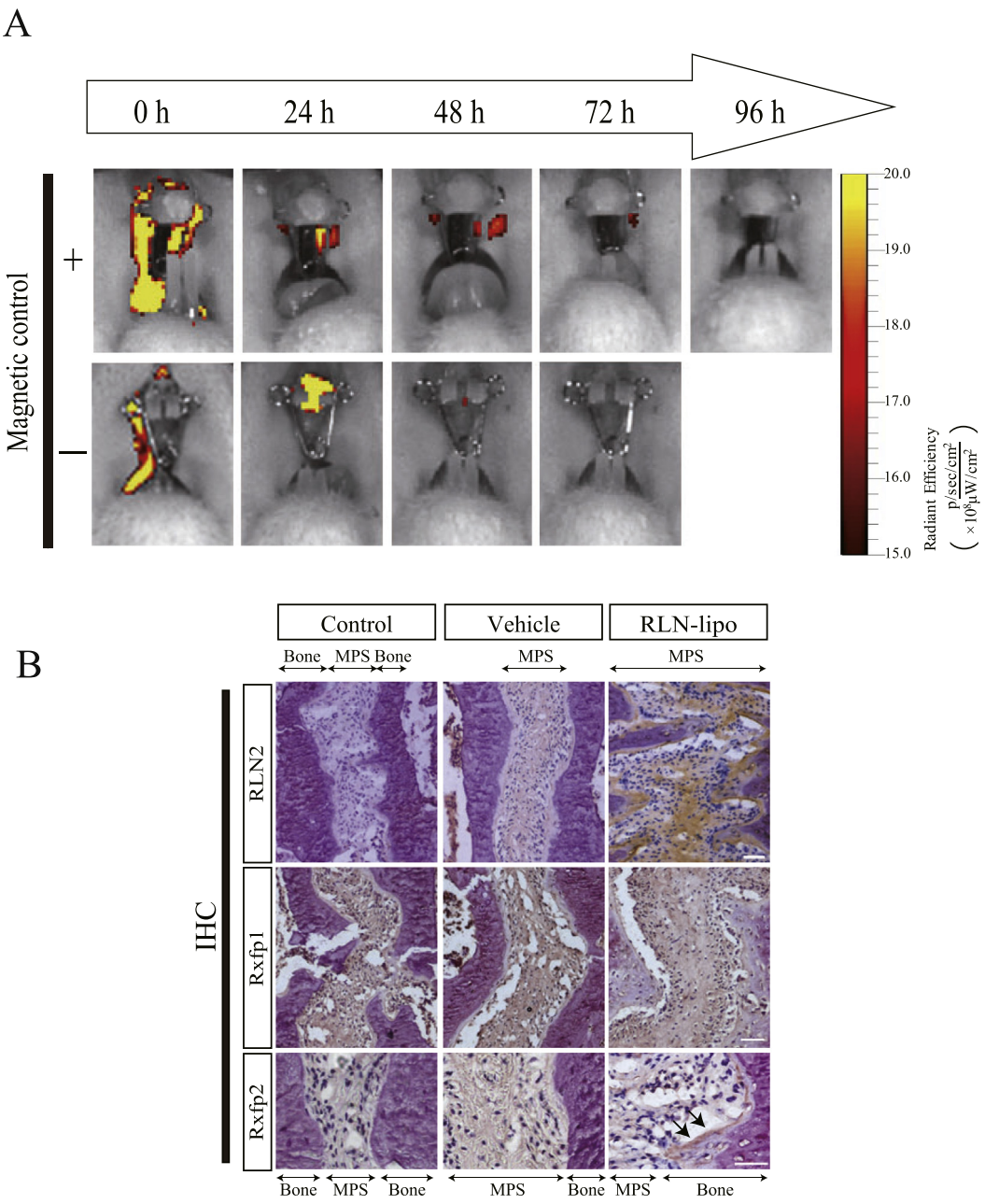

Fig. 2. *In vivo* imaging of administered liposomes and IHC of RLN2, RXFP1, and RXFP2.
(A) *In vivo* imaging of fluorescent Cy5.5 around the rat MPS by a preliminary examination. Warmer colors represent higher radiant efficiency. (B) IHC analysis of RLN2, RXFP1, and RXFP2 in the different groups. Arrows indicate Rxfp2-positive osteoblasts. Scale bar, 50 μm.

through the MPS only in the RLN-lipo group. These findings confirmed the presence of RLN2 owing to magnetically controlled liposomes in the MPS throughout the experimental period. Next, the expression of RXFP1 and RXFP2 was analyzed by IHC after expansion. Notably, RXFP1 was expressed in the MPS in all groups (Fig. 2B). Interestingly, RXFP2 expression was detected in osteoblasts at the osteogenic front of the RLN-lipo group only (Fig. 2B).

3.2. RLN2 promoted MPS expansion and MMP-1 and iNOS secretion in fibroblasts

Next, we assessed the effects of RLN2 on expansion efficiency using micro-CT analysis. In the RLN-lipo group, the MPS was clearly expanded (Fig. 3A). The distance of the mature alveolar bony edge was significantly larger in the RLN-lipo group than in the other groups (Fig. 3A), indicating that MPS expansion was greater in the RLN-lipo group. To explore the mechanisms mediating these effects, we performed fluorescent immunostaining. In the control group, MMP-1 expression was slightly increased in the vehicle group but was substantially stimulated in fibroblasts and osteoblasts in the MPS in the RLN-lipo group (Fig. 3B). The expression of iNos was not observed in the control or vehicle groups but was present in the RLN-lipo group (Fig. 3C).

3.3. RLN2 enhanced osteoblast proliferation, differentiation, and new bone formation at the osteogenic front of the MPS during expansion

In vitro application of RLN2-liposomes on primary cultured cells isolated from rat maxillary bone containing MPS enhanced the expression of *Runx2* mRNA, as determined by RT-PCR (Supplemental

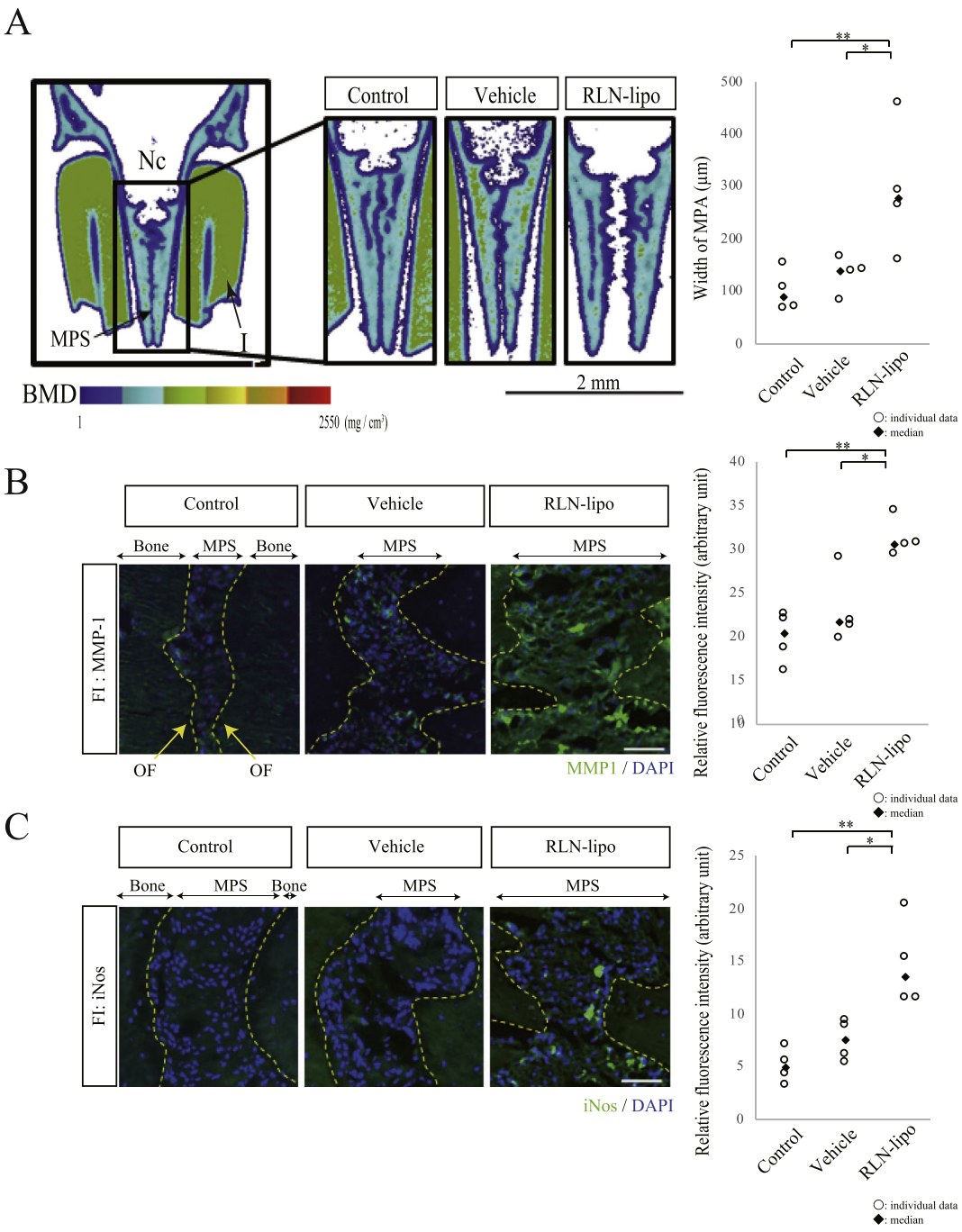

Fig. 3. Micro-CT images of MPS and expression of MMP-1 and iNOS after 7 days of expansion.
(A) Micro-CT images of coronal sections through MPS after 7 days of expansion. The newly formed area is shown in dark blue. Scale bar, 2.0 mm. I, upper incisors; Nc, nasal cavity. n = 4 for each group. (B, C) Fluorescent immunostaining (FI) of MMP-1 (B) and iNOS (C) (green). Yellow lines indicate the osteogenic front of the MPS. OF, osteogenic front. Scale bar in B and C, 50 μm. Individual data from the subjects are represented by open circles (○) and median values are indicated by closed rhombi (◆), and n = 4 for each group. $*p < 0.05$, $**p < 0.01$. (For interpretation of the references to color in this figure legend, the reader is referred to the web version of this article.)

Fig. 1). HE staining of the MPS after expansion and retention periods showed serrate bone formation only in the RLN-lipo group (Fig. 4A). Mature bone, newly formed bone, and fibroblasts in the mid-sutural area were obviously distinguishable, and the area of newly formed bone was significantly larger in the RLN-lipo group than in the other groups (Fig. 4B). No cartilage formation was observed around the MPS after expansion (data not shown). In the expansion group, osteoblasts lining the osteogenic front became aggregated along the osteogenic front, and there was a significant increase in the number of nuclei, particularly in the RLN-lipo group (Fig. 4C). Interestingly, assessment of apoptotic changes at the MPS after expansion revealed no apoptosis (data not shown). As we previously showed (Duarte et al., 2017), the number of osteoclast-like cells may be elevated in the RLN-lipo group. However, analysis of TRAP activity in the MPS after expansion revealed no evidence of osteoclast (data not shown). As previously reported (Wu et al., 2017), osteoclast may not have critical roles in bone remodeling during MPS expansion, although RLN increases the number of osteoclast during calvarial sagittal suture expansion (Duarte et al., 2017). Notably, using ALP activity assays, we found that osteoblast differentiation was limited to a thin, single line at the osteogenic front of the MPS in

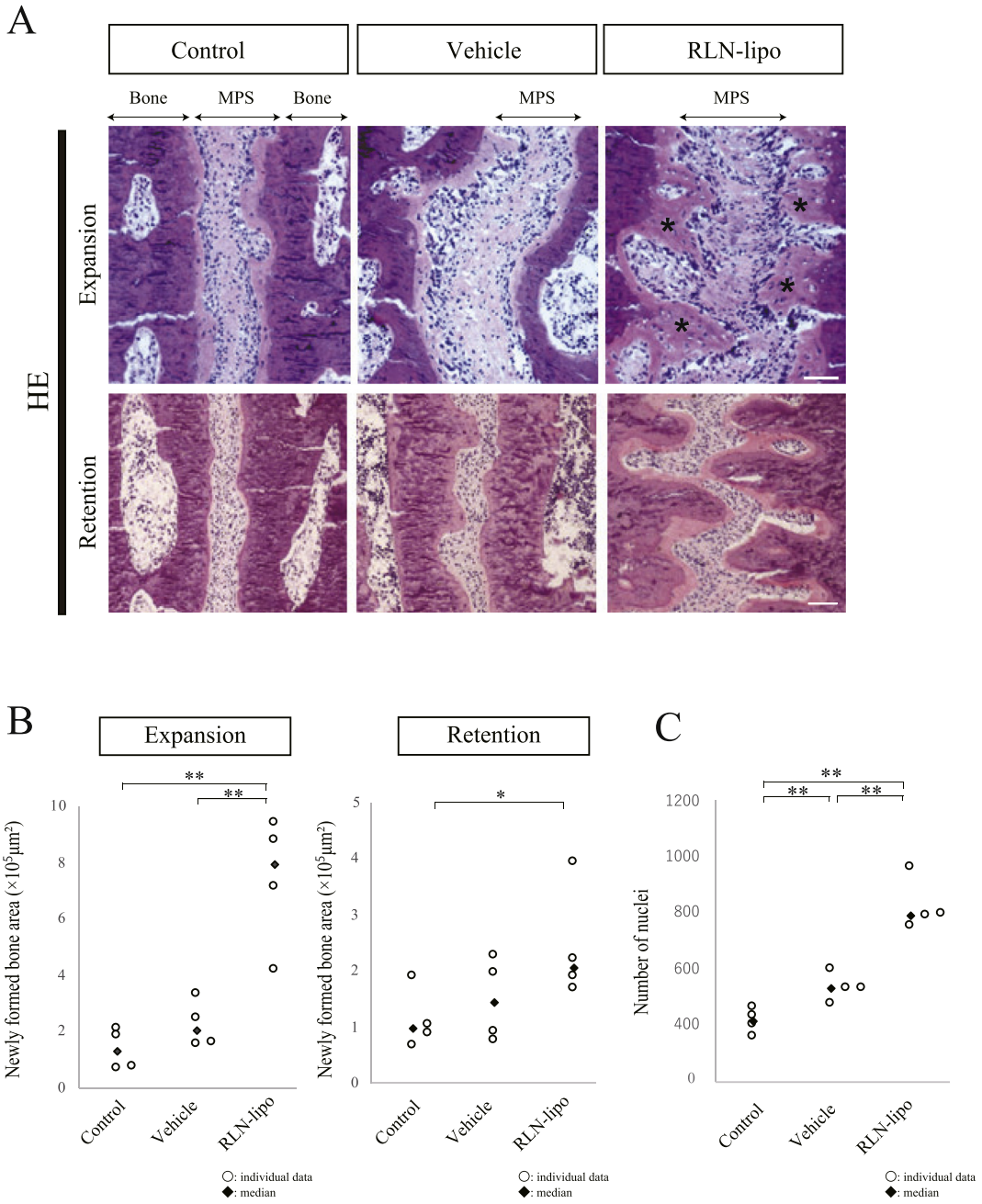

Fig. 4. Histological observation of MPS after expansion and retention.
(A) HE staining showing MPS width, the osteogenic front, and newly formed bone in the different groups. Newly formed bone is shown in pale pink (asterisks). (B) Newly formed bone area of expansion and retention groups were evaluated by NIH image software. (C) The number of nuclei was counted on the HE images, at the suture and newly formed bone area. Scale bar, 50 μm. Individual data from the subjects are represented by open circles (○) and median values are indicated by closed rhombi (◆), and n = 4 for each group. $*p < 0.05$, $**p < 0.01$. (For interpretation of the references to color in this figure legend, the reader is referred to the web version of this article.)

the control group (Fig. 5A). In the vehicle group, slight enlargement of the ALP-positive area was observed, possibly as a reaction to mechanical stress applied at the MPS. The ALP-positive area was significantly expanded in the RLN-lipo group (Fig. 5A). To assess the Mineral apposition rate (MAR), bone formation rate (BFR), and mineralizing surface/bone surface (MS/BS) at the MPS during expansion, we performed bone histomorphometric analysis. As shown in Fig. 5B, the MAR was significantly higher in the vehicle group than in the control group and in the RLN-lipo group than in the vehicle group. Thus, mechanical stress applied to the alveolar bone caused an osteogenic response, and RLN2 enhanced this effect in the MPS (Fig. 5B).

3.4. Acceleration of osteoblast differentiation and new bone formation by RLN2 via POSTN and SOST

Next, we analyzed the expression patterns of POSTN and SOST at the MPS. Interestingly, intense expression of POSTN was observed in osteoblasts at the osteogenic front of the MPS in the RLN-lipo group (Fig. 6A). Abundant SOST expression was observed in osteocytes in the alveolar bone in the control group, whereas downregulation of SOST was observed in the vehicle group (Fig. 6B). Osteocytes in the newly formed immature bone in the RLN-lipo group expressed significantly lower levels of SOST than other groups (Fig. 6B).

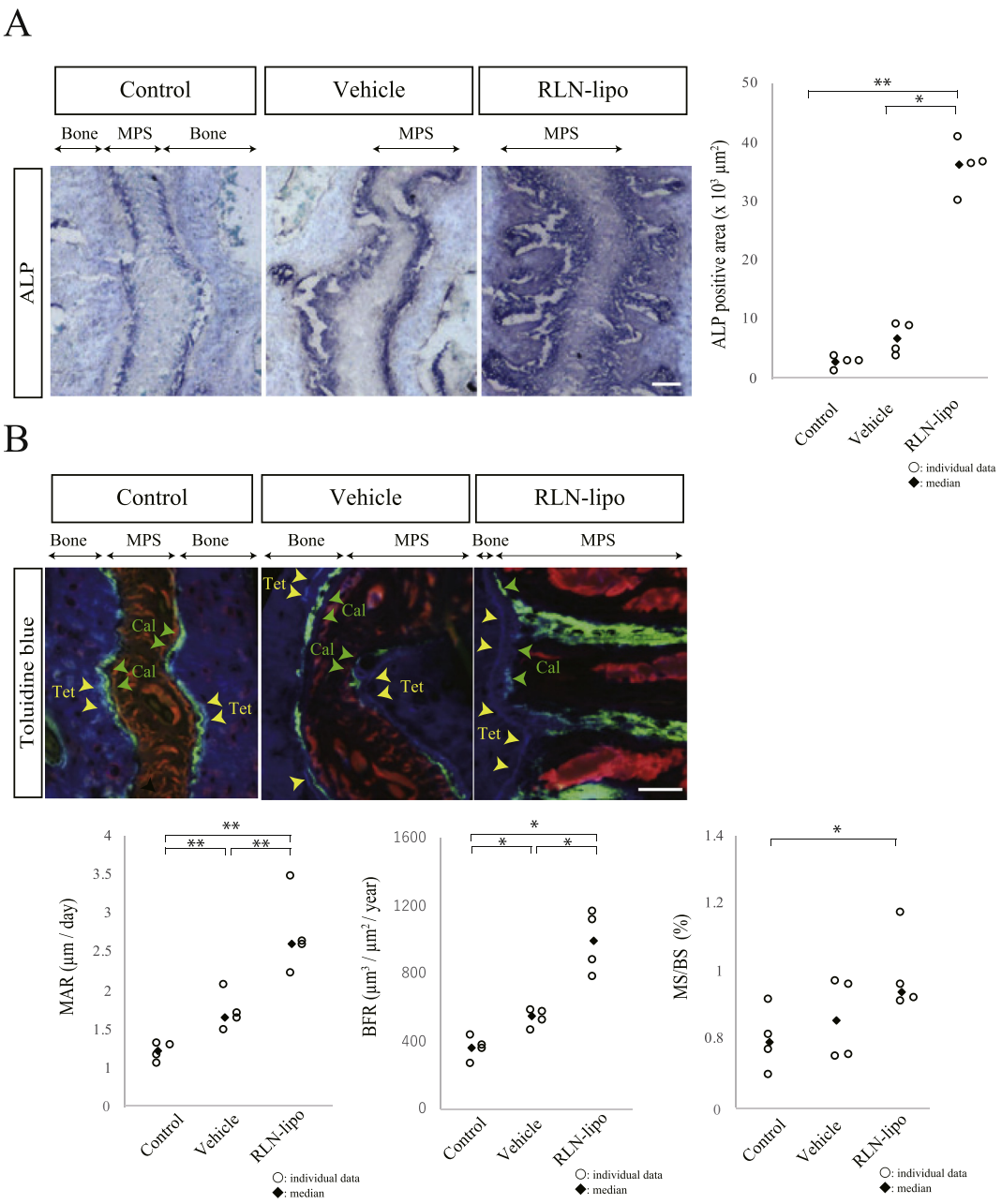

Fig. 5. Alkaline phosphatase (ALP) activity and bone double-labeling of MPS during expansion.
(A) ALP staining was performed on MPS after expansion. The ALP-positive area was stained dark purple. Quantification of the ALP-positive area was evaluated with NIH image software. (B) Bone histomorphometric analysis after expansion by the bone double-labeling method with tetracycline (Tet) and calcein (Cal). Mineral apposition rate (MAR), bone formation rate (BFR), and mineralizing surface/bone surface (MS/BS) for each group was evaluated on the toluidine blue staining images. Scale bar, 50 μm. Individual data from the subjects are represented by open circles (○) and median values are indicated by closed rhombi (◆), and n = 4 for each group. $*p < 0.05$, $**p < 0.01$. (For interpretation of the references to color in this figure legend, the reader is referred to the web version of this article.)

4. Discussion

Mesenchymal stem cells in the craniofacial suture have been reported to have important roles in bone development, homeostasis, repair, and regeneration and as a postnatal growth center (Maruyama et al., 2016; Zhao et al., 2015). The maxillary bones are of mesenchymal origin, derived from multipotent cranial neural crest cells, and are connected to each other by dense fibrous connections called the MPS. During infancy, the MPS is almost straight but changes shape over time; finally, interdigitation and bony bridging develop, making advanced that skeletal maxillary lateral expansion impossible by the late teens (Melsen, 1975). Therefore, adult orthodontic patients who present maxillary transverse deficiency sometimes require invasive surgically assisted palatal expansion to acquire the proper upper dental arch width. Additionally, long-term retention is needed to avoid unfavorable relapse after lateral expansion. Currently, there are no pharmacological approaches for the control of sutural growth, disease, and remodeling; therefore, effective and minimally invasive approaches for controlling these biological phenomena are needed. Accordingly, we have studied the effects of RLN in bone remodeling (Duarte et al., 2014a; Duarte et al., 2017) and found that RLN2 may enhance osteoblast differentiation, resulting in new bone formation after calvarial sagittal suture expansion (Duarte et al., 2014a). Here, we developed a unique magnetically controlled RLN2 delivery system, which enabled localization

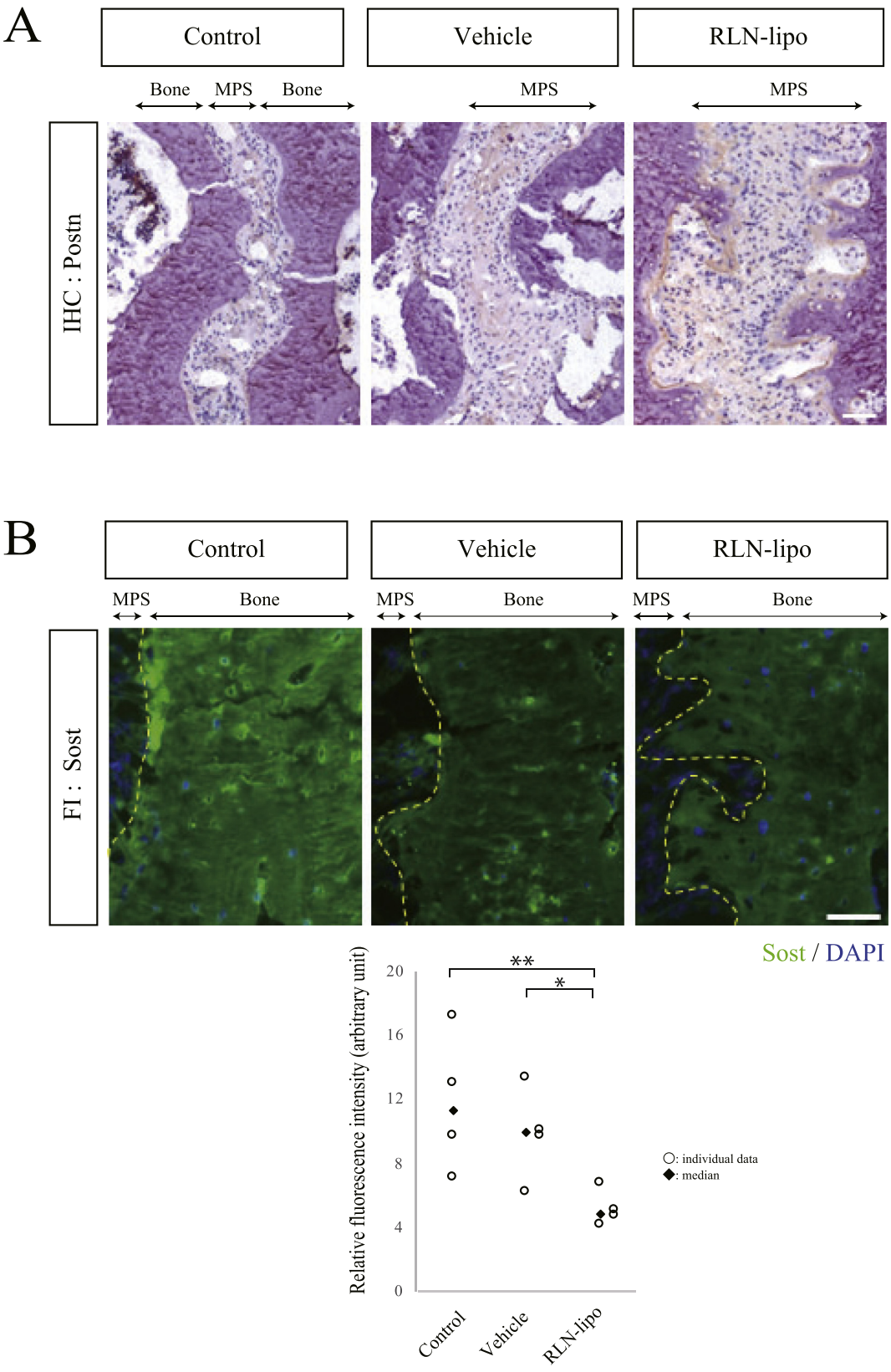

Fig. 6. POSTN and SOST expression in the MPS after expansion.
(A) IHC staining of POSTN (brown). (B) FI staining of SOST (green). Nuclei were stained with DAPI (blue). Scale bar, 50 μm. Individual data from the subjects are represented by open circles (○) and median values are indicated by closed rhombi (◆), and n = 4 for each group; error bars indicate standard deviations. *$p < 0.05$, **$p < 0.01$. (For interpretation of the references to color in this figure legend, the reader is referred to the web version of this article.)

of RLN2 into the MPS; we then analyzed the effects of RLN2 on MPS expansion.

High expression of RXFP1 has been observed in pathological conditions, such as liver fibrosis (McBride et al., 2017). Here, we found abundant expression of RXFP1 in sutural fibroblasts in the MPS, regardless of the expansion force applied and RLN2 administration. RLN2 signal is transduced through RXFP1 to activate ERK1/2 phosphorylation and an nNOS/NO/cGMP-dependent pathway in human renal myofibroblasts, thereby inhibiting Smad2 phosphorylation and blocking TGF-β1 activity (Heeg et al., 2005). This pathway mediates myofibroblast differentiation and myofibroblast-derived aberrant collagen production (Heeg et al., 2005). Moreover, Chow et al. demonstrated that H2 relaxin activates not only an RXFP1/phospho-ERK/nNOS/NO/cGMP-dependent pathway to mediate its antifibrotic effects but also iNOS to promote MMP expression which is associated with collagen degradation (Chow et al., 2012). Furthermore, by suppressing the TGF-β1/phospho-Smad2 axis, which inhibits iNOS activity in myofibroblasts, H2 relaxin can release iNOS, contributing to MMP-promoting effects (Chow et al., 2012). Consistent with these findings, we found that RLN2 signaled through RXFP1, which was abundantly expressed in sutural fibroblasts, to promote MMP-1 expression. MMP-2 expression, tissue inhibitor of metalloproteinases (TIMP)-1 expression, and the MMP-2/TIMP-1 ratio are significantly enhanced during rat MPS expansion (Chen et al., 2017). Additionally, serelaxin inhibits TGF-β1-induced cardiac fibroblast differentiation towards myofibroblasts, reduces the production of collagens by inhibiting the ALK-5/Smad2/3 signaling pathway, and enhances extracellular matrix degradation by increasing the MMP-2/TIMP-2 ratio and interleukin-10 secretion (Wu et al., 2018).

Relaxin and relaxin-related hormones, such as INSL3, contribute to the establishment of sex differences under pathological conditions of the skeletal tissue, such as osteoporosis and sarcopenia (Ferlin et al., 2017). Ferlin et al. showed that mutation of the *RXFP2* gene causes significantly reduced bone mineral density (Ferlin et al., 2008) and that treatment of human and mouse osteoblasts expressing RXFP2 with INSL3 promotes cAMP production to affect cell proliferation. Similarly, RXFP2-deficient mice show decreased bone mass, mineralizing surface, bone formation, and osteoclast surface compared with wild-type littermates (Ferlin et al., 2011), suggesting that INSL3/RXFP2 signaling has an important role in bone and mineral metabolism *in vivo* and linking *RXFP2* gene mutations with human osteoporosis (Ferlin et al., 2008). In contrast, RLN enhances BMP2-induced bone formation and osteoblast differentiation in mouse bone marrow stem cells and mouse embryonic C3H/10T1/2 fibroblasts through RXFP1 by augmenting and sustaining Smad and p38 phosphorylation, resulting in enhancement of Runx2 expression and its activity (Moon et al., 2014). In this study, we found significantly increased serrate bone deposition with RLN2 administration during the active expansion and retention period. Some reports showed bone formation after rat MPS expansion by tooth-borne appliances (Buyuk et al., 2016; Chen et al., 2017; Sadikoglu et al., 2016). Wu et al. reported that the “finger-like” pattern of newly formed bone was caused by interruption of the relatively heavy expansion force in the MPS (Wu et al., 2017). We speculate that disbalance of the mechanical stress caused by the degradation of collagen fibrils in the MPS creates this morphology. In addition, *Rxfp1* and *Rxfp2* mRNAs are expressed in the developing calvarial frontal bones and facial bones (Duarte et al., 2014a). RLN has also been shown to enhance osteoblastic differentiation, mediated by enhanced Runx2 expression and subsequent upregulation of ALP activity; these changes were accompanied by ERK1/2 phosphorylation through RXFP2 in MC3T3-E1 mouse calvarial osteoblasts, thereby enhancing *in vitro* mineralization (Duarte et al., 2014a). We have previously reported that Rxfp1 and Rxfp2 are expressed in developing bone and that RLN influences bone metabolism by binding to Rxfp2. This effect might be regulated by Rxfp1, the expression of which is induced during osteoblast differentiation (Duarte et al., 2014a). Moreover, RLN affects osteoblast mineralization owing to its capacity to increase the activities of MMP2 and MMP-13 in osteoblasts (Duarte et al., 2014a). Overall, we propose that RLN2 exhibits osteogenic effects through RXFP2, which is upregulated by administration of RLN2.

Interestingly, POSTN upregulation in osteoblasts was observed only in the RLN-lipo group. The matricellular protein POSTN is expressed in collagen-rich tissues subjected to continuous mechanical loading, such as the periodontal ligament, periosteum, and alveolar bone surface in adult tissue (Kii and Kudo, 2007). POSTN mediates bone modeling in response to mechanical stress (Moriyama, 2012; Wilde et al., 2003) and activates Wnt/β-catenin signaling directly and through downregulation of SOST by intermittent PTH stimulation (Bonnet et al., 2009). Recent studies have shown that POSTN is a substrate of cathepsin K (CTSK) and that inhibition of CTSK increases POSTN levels at the periosteum and in osteocytes, resulting in Wnt/β-catenin activation and new cortical bone formation (Bonnet et al., 2017). Thus, POSTN is thought to be an important activator of periosteal bone modeling. Additionally, SOST was found to be downregulated in the vehicle group, presumably owing to mechanical stress applied during the expansion. Notably, weak SOST expression was observed in osteocytes in the newly formed bone in the RLN-lipo group. Targeted deletion of SOST results in increased bone formation and bone strength (Li et al., 2008). The molecular mechanisms through which osteocytes sense and transduce mechanical stress to alter SOST expression remain unclear but may involve interactions with POSTN. POSTN expression is required for SOST inhibition and is important for determination of bone mass changes in response to mechanical loading (Bonnet et al., 2009). In the present study, RLN2 treatment influenced SOST and POSTN expression in MPS and palatal bones, although no direct or indirect evidence to link RLN2 with either of these two molecules has been elucidated. It is speculated that ERK signaling pathway might be a possible candidate to induce these phenomena because it is known to be activated *via* RLN/Rxfp signal in osteoblastic cells (Duarte et al., 2014a). To prove the precise molecular mechanism to induce SOST and POSTN expression in MPS and palatal bones, further *in vivo* and *in vitro* studies will be needed. Taken together, magnetically directed RLN2 carried by liposomes were found to be a unique, effective method for suture expansion. Our data revealed that RLN2 enhanced suture expansion *via* MMP-1 secretion in the sutural fibroblasts and new bone formation *via* POSTN expression in osteoblasts at the osteogenic front. These properties may be useful for developing unique strategies for less-invasive and effective orthopedic treatment in craniofacial and maxillofacial sutures.

Supplementary data to this article can be found online at https://doi.org/10.1016/j.bonr.2019.100202.

Disclosure

The authors declare no conflicts of interest associated with this manuscript.

Transparency document

The Transparency document associated with this article can be found, in the online version.

Acknowledgements

This work was supported by Japan Society for the Promotion of Science (JSPS) KAKENHI Grant Number JP16K11779 and JP25463168 to YK, and JP26253093 to KM.

References

Baccaglini, L., Shamsul Hoque, A.T., Wellner, R.B., Goldsmith, C.M., Redman, R.S., Sankar, V., Kingman, A., Barnhart, K.M., Wheeler, C.J., Baum, B.J., 2001. Cationic liposome-mediated gene transfer to rat salivary epithelial cells in vitro and in vivo. J

Gene Med 3 (1), 82–90.
Barron, M.A., Lay, M., Madinger, N.E., 2005. Surgery and treatment with high-dose liposomal amphotericin B for eradication of craniofacial zygomycosis in a patient with Hodgkin's disease who had undergone allogeneic hematopoietic stem cell transplantation. J. Clin. Microbiol. 43 (4), 2012–2014.
Bathgate, R.A., Ivell, R., Sanborn, B.M., Sherwood, O.D., Summers, R.J., 2005. Receptors for relaxin family peptides. Ann. N. Y. Acad. Sci. 1041, 61–76.
Bathgate, R.A., Lin, F., Hanson, N.F., Otvos, L., Jr., Guidolin, A., Giannakis, C., Bastiras, S., Layfield, S.L., Ferraro, T., Ma, S., et al. 2006. Relaxin-3: improved synthesis strategy and demonstration of its high-affinity interaction with the relaxin receptor LGR7 both in vitro and in vivo. Biochemistry 45 (3), 1043–1053.
Bathgate, R.A., Halls, M.L., van der Westhuizen, E.T., Callander, G.E., Kocan, M., Summers, R.J., 2013. Relaxin family peptides and their receptors. Physiol. Rev. 93 (1), 405–480.
Bonnet, N., Standley, K.N., Bianchi, E.N., Stadelmann, V., Foti, M., Conway, S.J., Ferrari, S.L., 2009. The matricellular protein periostin is required for sost inhibition and the anabolic response to mechanical loading and physical activity. J. Biol. Chem. 284 (51), 35939–35950.
Bonnet, N., Brun, J., Rousseau, J.C., Duong, L.T., Ferrari, S.L., 2017. Cathepsin K controls cortical bone formation by degrading periostin. J. Bone Miner. Res. 32 (7), 1432–1441.
Buyuk, S.K., Ramoglu, S.I., Sonmez, M.F., 2016. The effect of different concentrations of topical ozone administration on bone formation in orthopedically expanded suture in rats. Eur. J. Orthod. 38 (3), 281–285.
Chen, J., Zhou, J., Li, F., Sun, J., Li, G., Zou, S., Ye, Q., 2017. Expression of MMP-2 and TIMP-1 during rapid maxillary expansion in rats. Arch. Oral Biol. 76, 30–35.
Chow, B.S., Chew, E.G., Zhao, C., Bathgate, R.A., Hewitson, T.D., Samuel, C.S., 2012. Relaxin signals through a RXFP1-pERK-nNOS-NO-cGMP-dependent pathway to up-regulate matrix metalloproteinases: the additional involvement of iNOS. PLoS One 7 (8), e42714.
Duarte, C., Kobayashi, Y., Kawamoto, T., Moriyama, K., 2014a. RELAXIN enhances differentiation and matrix mineralization through Relaxin/insulin-like family peptide receptor 2 (Rxfp2) in MC3T3-E1 cells in vitro. Bone 65, 92–101.
Duarte, C., Kobayashi, Y., Kawamoto, T., Moriyama, K., 2014b. Relaxin receptors 1 and 2 and nuclear receptor subfamily 3, group C, member 1 (glucocorticoid receptor) mRNAs are expressed in oral components of developing mice. Arch. Oral Biol. 59 (2), 111–118.
Duarte, C., Kobayashi, Y., Morita, J., Kawamoto, T., Moriyama, K., 2017. A preliminary investigation of the effect of relaxin on bone remodelling in suture expansion. Eur. J. Orthod. 39 (3), 227–234.
Ferlin, A., Pepe, A., Gianesello, L., Garolla, A., Feng, S., Giannini, S., Zaccolo, M., Facciolli, A., Morello, R., Agoulnik, A.I., et al. 2008. Mutations in the insulin-like factor 3 receptor are associated with osteoporosis. J. Bone Miner. Res. 23 (5), 683–693.
Ferlin, A., Perilli, L., Gianesello, L., Taglialavoro, G., Foresta, C., 2011. Profiling insulin like factor 3 (INSL3) signaling in human osteoblasts. PLoS One 6 (12), e29733.
Ferlin, A., De Toni, L., Sandri, M., Foresta, C., 2017. Relaxin and insulin-like peptide 3 in the musculoskeletal system: from bench to bedside. Br. J. Pharmacol. 174 (10), 1015–1024.
He, D., Kou, X., Yang, R., Liu, D., Wang, X., Luo, Q., Song, Y., Liu, F., Yan, Y., Gan, Y., et al. 2015. M1-like macrophage polarization promotes orthodontic tooth movement. J. Dent. Res. 94 (9), 1286–1294.
Heeg, M.H., Koziolek, M.J., Vasko, R., Schaefer, L., Sharma, K., Muller, G.A., Strutz, F., 2005. The antifibrotic effects of relaxin in human renal fibroblasts are mediated in part by inhibition of the Smad2 pathway. Kidney Int. 68 (1), 96–109.
Kii, I., Kudo, A., 2007. Periostin function in the periodontal ligament and the periosteum. Clin Calcium 17 (2), 202–208.
Li, X., Ominsky, M.S., Niu, Q.T., Sun, N., Daugherty, B., D'Agostin, D., Kurahara, C., Gao, Y., Cao, J., Gong, J., et al. 2008. Targeted deletion of the sclerostin gene in mice results in increased bone formation and bone strength. J. Bone Miner. Res. 23 (6), 860–869.
Lu, C., Lam, H.N., Menon, R.K., 2005. New members of the insulin family: regulators of metabolism, growth and now … reproduction. Pediatr. Res. 57 (5 Pt 2), 70R–73R.
Maruyama, T., Jeong, J., Sheu, T.J., Hsu, W., 2016. Stem cells of the suture mesenchyme in craniofacial bone development, repair and regeneration. Nat. Commun. 7, 10526.
Matsuo, T., Sugita, T., Kubo, T., Yasunaga, Y., Ochi, M., Murakami, T., 2003. Injectable magnetic liposomes as a novel carrier of recombinant human BMP-2 for bone formation in a rat bone-defect model. J. Biomed. Mater. Res. A 66 (4), 747–754.
McBride, A., Hoy, A.M., Bamford, M.J., Mossakowska, D.E., Ruediger, M.P., Griggs, J., Desai, S., Simpson, K., Caballero-Hernandez, I., Iredale, J.P., et al. 2017. In search of a small molecule agonist of the relaxin receptor RXFP1 for the treatment of liver fibrosis. Sci. Rep. 7 (1), 10806.
Melsen, B., 1975. Palatal growth studied on human autopsy material. A histologic microradiographic study. Am. J. Orthod. 68 (1), 42–54.
Mookerjee, I., Hewitson, T.D., Halls, M.L., Summers, R.J., Mathai, M.L., Bathgate, R.A., Tregear, G.W., Samuel, C.S., 2009. Relaxin inhibits renal myofibroblast differentiation via RXFP1, the nitric oxide pathway, and Smad2. FASEB J. 23 (4), 1219–1229.
Moon, J.S., Kim, S.H., Oh, S.H., Jeong, Y.W., Kang, J.H., Park, J.C., Son, H.J., Bae, S., Park, B.I., Kim, M.S., et al. 2014. Relaxin augments BMP-2-induced osteoblast differentiation and bone formation. J. Bone Miner. Res. 29 (7), 1586–1596.
Moriyama, K., 2012. Periostin: a multifunctional matricellular protein refocused in dental science. Japanese Dental Science Review 48 (2), 99–100.
Sadikoglu, T.B., Nalbantgil, D., Ulkur, F., Ulas, N., 2016. Effect of hyaluronic acid on bone formation in the expanded interpremaxillary suture in rats. Orthod Craniofac Res 19 (3), 154–161.
Wilde, J., Yokozeki, M., Terai, K., Kudo, A., Moriyama, K., 2003. The divergent expression of periostin mRNA in the periodontal ligament during experimental tooth movement. Cell Tissue Res. 312 (3), 345–351.
Wu, B.H., Kou, X.X., Zhang, C., Zhang, Y.M., Cui, Z., Wang, X.D., Liu, Y., Liu, D.W., Zhou, Y.H., 2017. Stretch force guides finger-like pattern of bone formation in suture. PLoS One 12 (5).
Wu, X.P., Wang, H.J., Wang, Y.L., Shen, H.R., Tan, Y.Z., 2018. Serelaxin inhibits differentiation and fibrotic behaviors of cardiac fibroblasts by suppressing ALK-5/Smad2/3 signaling pathway. Exp. Cell Res. 362 (1), 17–27.
Zhao, H., Feng, J., Ho, T.V., Grimes, W., Urata, M., Chai, Y., 2015. The suture provides a niche for mesenchymal stem cells of craniofacial bones. Nat. Cell Biol. 17 (4), 386–396.